SINGULARITIES OF CAPILLARY-GRAVITY WAVES ON DIELECTRIC FLUID UNDER NORMAL ELECTRIC FIELDS[*]

TAO GAO[†], ZHAN WANG[‡], AND DEMETRIOS PAPAGEORGIOU[§]

Abstract. As summarized by Papageorgiou (*Annu. Rev. Fluid Mech.*, vol. 51, 2019, pp. 155–187), a strong normal electric field can cause instability of the interface in a hydrodynamic system. In the present work, singularities arising in electrocapillary-gravity waves on a dielectric fluid of finite depth due to an electric field imposed in the direction perpendicular to the undisturbed free surface are investigated. In shallow water, for a small-amplitude periodic disturbance in the linearly unstable regime, the outcome of the system evolution is that the gas-liquid interface touches the solid bottom boundary, causing a rupture. A quasi-linear hyperbolic model is derived for the long-wave limit and used to study the formation of the touch-down singularity. The theoretical predictions are compared with the fully nonlinear computations by a time-dependent conformal mapping for the electrified Euler equations, showing good agreement. On the other hand, a nonlinear dispersive model system is derived for the deep-water scenario, which predicts the blowup singularity (i.e., the wave amplitude tends to infinity in a finite time). However, when the fluid thickness is significantly large, one can numerically show the self-intersection non-physical wave structure or 2/3 power cusp singularity in the full Euler equations.

Key words. capillary-gravity, surface waves, singularity, electrohydrodynamics

AMS subject classifications. 15A15, 15A09, 15A23

1. Introduction. Electrohydrodynamics (EHD) is a cross-disciplinary subject concerned with interactions between fluid motion and electric field. It has been studied intensively in many different contexts by applied mathematicians, fluid dynamicists, and engineers due to its practical importance in the modern industry (see, for example, [10, 12]). In particular, EHD usually deals with an interface between two different fluids, which is a free boundary problem and, therefore, mathematically challenging. A decent understanding of interfacial waves under the effect of an electric field can significantly benefit relevant disciplinary communities.

The study of EHD interfacial waves was initiated by Taylor & McEwan [21]. The authors showed theoretically and experimentally that normal electric fields (the direction of the applied electric field is perpendicular to the undisturbed interface) could destabilize the interface between a dielectric and a conducting fluid. Later, a linear stability analysis of the problem under tangential electric fields (the direction of the applied electric field is parallel to the undisturbed interface) was conducted by Melcher & Schwarz [15]. It was shown in that paper that the electric force could regularize short waves. These two pioneering works illustrate the effects of electric fields on linear interfacial waves in the inviscid limit.

The research of EHD waves was later extended to nonlinear regimes. The long-wave approximation was most commonly examined in the literature, and the method of multiple scales was employed for analyses. In these reduced models, a touching singularity, i.e., the interface touches the rigid wall, is usually observed. For tangential electric fields, the rupture and touching singularity were numerically found in long-wave models in liquid films [22] and interfacial electrocapillary-gravity waves [2], respectively. While for normal electric fields, the touching singularity was shown to exist by Papageorgiou *et al.* [19] for interfacial waves between two dielectrics with a hydrodynamically passive gas on top of a thin liquid layer.

More recently, Gao *et al.* [7, 8] conducted numerical experiments for the electrified Euler equations on the time evolution of the interface between an active dielectric liquid and a passive conducting gas. Gao *et al.* [9] followed to study the nonlinear wave interactions in the same physical configuration and derived a number of useful model equations in this context. In particular, numerical evidence for the touch-down singularity was shown by [7]; however, the mechanism of

[†]Department of Mathematical Sciences, University of Essex, Colchester CO4 3 SQ, UK (`t.gao@essex.ac.uk`).

[‡]Institute of Mechanics, Chinese Academy of Sciences, Beijing 100190, PR China (`zwang@imech.ac.cn`), and School of Engineering Sciences, University of Chinese Academy of Sciences, Beijing 100049, PR China.

[§]Department of Mathematics, Imperial College London, South Kensington, London SW7 2AZ, UK (`d.papageorgiou@imperial.ac.uk`).
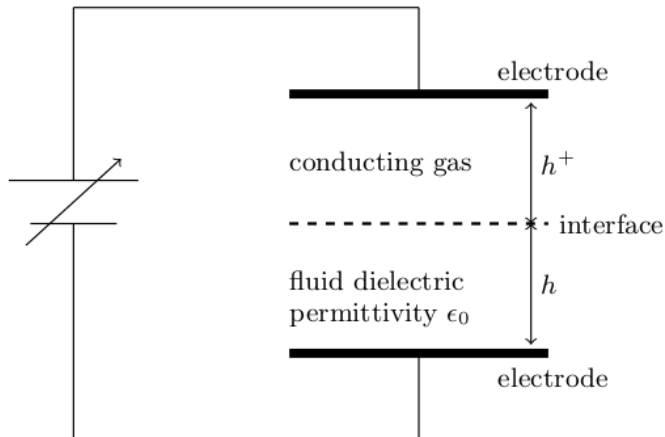
FIG. 2.1. *Schematic of the problem. The electric potential difference between two electrodes is a constant.*

singularity formation has not been thoroughly investigated. More importantly, the existence of touching singularity seems to depend on the thickness of the liquid layer, and it becomes difficult for the interface to touch the wall when the fluid is considerably deep. As an extreme example, Kochurin *et al.* [13] showed the curvature singularity (blowup of the second derivative) and cusp singularity (blowup of the first derivative) appearing on the interface between two semi-infinite dielectrics within the limit of strong normal electric fields. Their results were obtained using reduced quadratic models with different permittivity and density ratios. On the other hand, other special physical processes may occur before forming the singularities mentioned above and hence halt the further evolution of the system; for instance, the self-intersection structure enclosing air bubbles due to the capillary effect in small-scale water waves. These intuitions motivate us to explore the singularities and dynamics in different depths of fluids with the electrified Euler equations. For other physical configurations such as dielectric gas and conducting fluid or dielectric gas and dielectric fluid, the touch-down may also occur, as shown by the numerical evidence in [19]. A full investigation will be conducted in future work.

We conduct numerical experiments for the electrified Euler equations in the present work based on the same configuration as [7], namely a dielectric of finite depth bounded above by a perfectly conducting and hydrodynamically passive gas ([7]) or liquid helium charged by electrons localized above its surface ([26]). The purpose of the paper is twofold: to understand the mechanism of the touching singularity in shallow fluid and singularity transition from shallow to deep fluids (i.e., the appearance and disappearance of rupture). The rest of the paper is structured as follows. The mathematical formulation of the problem, together with its Hamiltonian formulation, is described in §2. Reduced nonlinear models are derived in §3 in the shallow-water and deep-water limits, respectively, via the asymptotic analyses of the Hamiltonian. The numerical scheme for the primitive equations, the time-dependent conformal mapping, is introduced in §4. In §5, the theoretical results of the reduced models are compared with those of the electrified Euler equations. Finally, a conclusion is given in §6.

2. Mathematical Formulation.

2.1. Governing equations. We consider an incompressible and inviscid fluid of depth h in a two-dimensional $x - y$ Cartesian coordinate system. The forces due to surface tension σ and gravitational acceleration g are present – the latter acts in the negative y-direction. The fluid is bounded below by a rigid wall and above by a hydrodynamically passive gas of depth h^+. The interface between gas and liquid is usually referred to as the free surface, which is deformed by waves propagating in the x-direction denoted by $y = \zeta(x, t)$, with t being the time variable.

Without loss of generality, we choose the mean level of the free surface to be $y = 0$ and, therefore, the bottom is at $y = -h$. An electric field is imposed following the positive y-direction, i.e., perpendicular to the undisturbed free surface, by setting two electrodes on the top and bottom, respectively, with a difference in voltage potential, which is always a constant. We denote by v the voltage potential and let $v = -V_0$ at the bottom and $v = 0$ at the top. The fluid is assumed to be a dielectric with permittivity ϵ_0, whereas the gas is perfectly conducting. A schematic of the problem is sketched in Figure 2.1. The fluid motion is supposed to be irrotational; hence there exists a potential function ϕ such that the velocity field is its gradient. Following [8], the governing equations and boundary conditions read

$$(2.1) \qquad \nabla^2 \phi = 0, \qquad\qquad\qquad \text{for} \quad y < \zeta(x,t),$$

$$(2.2) \qquad \nabla^2 v = 0, \qquad\qquad\qquad \text{for} \quad y < \zeta(x,t),$$

$$(2.3) \qquad \zeta_t = \phi_y - \phi_x \zeta_x, \qquad\qquad \text{on} \quad y = \zeta(x,t),$$

$$(2.4) \qquad v = 0, \qquad\qquad\qquad\quad \text{for} \quad y \geqslant \zeta(x,t),$$

$$(2.5) \qquad v = -V_0, \qquad\qquad\qquad \text{on} \quad y = -h,$$

$$(2.6) \qquad \phi_y = 0, \qquad\qquad\qquad\quad \text{on} \quad y = -h,$$

and

$$(2.7) \qquad \phi_t + \frac{1}{2}|\nabla\phi|^2 + g\zeta - \frac{\sigma}{\rho}\kappa + \frac{\epsilon_0}{2\rho}|\nabla v|^2 = 0, \qquad \text{on} \quad y = \zeta(x,t),$$

where ρ is the fluid density, the subscripts denote partial derivatives, and $\kappa = \zeta_{xx}(1 + \zeta_x^2)^{-\frac{3}{2}}$ is the curvature. The last three terms of equation (2.7) are the forces due to gravity, surface tension, and Maxwell stresses resulting from the electric field. The electric term in (2.7) has been simplified by making use of (2.4) as shown in [8, 23]. Equations (2.3) and (2.6) are the kinematic boundary condition on the free surface and the impermeability condition at the bottom, respectively. By [7], the associated linear dispersion relation takes the form of

$$(2.8) \qquad \omega^2 = g|k| - \frac{\epsilon_0 V_0^2}{\rho h^2}k^2 + \frac{\sigma}{\rho}|k|^3,$$

where ω is the angular frequency and k is the wavenumber. When the right-hand side of (2.8) becomes negative, the fluid system is linearly unstable, resulting in the formation of singularities which will be investigated later on for various fluid depths.

2.2. Hamiltonian structure. In this section, we prove that equations (2.3) and (2.7) form a Hamiltonian system, provided (2.1)–(2.2) and (2.4)–(2.6) hold. In the absence of the electric field, it was Zakharov [25] who first published the Hamiltonian structure of the free-surface water-wave problem. In Zakharov's seminal work, the Hamiltonian is the total energy, and the surface displacement and velocity potential on the free surface form a pair of canonical variables. It is noted that the voltage potential can be uniquely determined by ζ provided the Dirichlet boundary conditions are given; thus, we can reasonably speculate that the canonical variables remain the same when the electric field is included. Defining $\varphi(x,t) = \phi(x, \zeta(x,t), t)$, we will show in the subsequent analysis that

(2.9)
$$\mathbb{H}[\zeta, \varphi] = \underbrace{\frac{1}{2}\int_{\mathbb{R}}\int_{-h}^{\zeta}|\nabla\phi|^2\mathrm{d}y\mathrm{d}x}_{\text{kinetic energy}} + \underbrace{\frac{g}{2}\int_{\mathbb{R}}\zeta^2\mathrm{d}x}_{\text{gravity}} - \underbrace{\frac{\epsilon_0}{2\rho}\int_{\mathbb{R}}\int_{-h}^{\zeta}|\nabla v|^2\mathrm{d}y\mathrm{d}x}_{\text{electric potential energy}} + \underbrace{\frac{\sigma}{\rho}\int_{\mathbb{R}}\left(\sqrt{1+\zeta_x^2} - 1\right)\mathrm{d}x}_{\text{capillarity}}$$

is the Hamiltonian with the canonical equations

$$(2.10) \qquad \zeta_t = \frac{\delta\mathbb{H}}{\delta\varphi}, \qquad \varphi_t = -\frac{\delta\mathbb{H}}{\delta\zeta},$$

which are equivalent to equations (2.3) and (2.7). For this purpose, it suffices to calculate the variational derivative of the electric potential energy with respect to ζ. We consider a small increment $\delta\zeta$ in the free surface ζ, and $\overline{v}(x, y, t)$ is the corresponding electric potential solved with the new surface $\zeta + \delta\zeta$ and the same Dirichlet boundary conditions (2.4)–(2.5). Thus by definition,

$$
(2.11)
\begin{aligned}
\delta \int_{\mathbb{R}} \int_{-h}^{\zeta} |\nabla v|^2 \mathrm{d}y\mathrm{d}x &= \int_{\mathbb{R}} \int_{-h}^{\zeta+\delta\zeta} |\nabla \overline{v}|^2 \mathrm{d}y\mathrm{d}x - \int_{\mathbb{R}} \int_{-h}^{\zeta} |\nabla v|^2 \mathrm{d}y\mathrm{d}x \\
&= \int_{\mathbb{R}} \delta\zeta \left(|\nabla v|^2\right)_{y=\zeta} \mathrm{d}x + \int_{\mathbb{R}} \int_{-h}^{\zeta} \left(|\nabla \overline{v}|^2 - |\nabla v|^2\right) \mathrm{d}y\mathrm{d}x \\
&= \int_{\mathbb{R}} \delta\zeta \left(|\nabla v|^2\right)_{y=\zeta} \mathrm{d}x + 2 \int_{\mathbb{R}} \left(\delta v \frac{\partial v}{\partial \mathbf{n}}\right)_{y=\zeta} \sqrt{1+\zeta_x^2}\, \mathrm{d}x,
\end{aligned}
$$

while retaining the leading order terms, where $\delta v = \overline{v}(x, y, t) - v(x, y, t)$ and $\mathbf{n} = (-\zeta_x, 1)/\sqrt{1+\zeta_x^2}$ is the unit normal vector of the free surface. It follows from $v(x, \zeta, t) = 0$ and $\overline{v}(x, \zeta + \delta\zeta, t) = 0$ that $\delta v(x, \zeta, t) = -v_y \delta\zeta$ to leading order. Substituting the above relation into equation (2.11) yields

$$
(2.12) \quad \delta \int_{\mathbb{R}} \int_{-h}^{\zeta} |\nabla v|^2 \mathrm{d}y\mathrm{d}x = \int_{\mathbb{R}} \delta\zeta \left[|\nabla v|^2 - 2v_y(v_y - \zeta_x v_x)\right]_{y=\zeta} \mathrm{d}x = -\int_{\mathbb{R}} \delta\zeta \left(|\nabla v|^2\right)_{y=\zeta} \mathrm{d}x,
$$

where $v_x + \zeta_x v_y = 0$ (because v is identically zero on the surface) at $y = \zeta$ has been used. Thus,

$$
(2.13) \qquad \varphi_t = -\frac{\delta \mathbb{H}}{\delta \zeta} = \frac{1}{2}\left(\phi_y^2 - \phi_x^2\right) - \zeta_x \phi_x \phi_y - g\zeta - \frac{\epsilon_0}{2\rho}|\nabla v|^2 + \frac{\sigma}{\rho}\frac{\zeta_{xx}}{(1+\zeta_x^2)^{3/2}},
$$

and we complete the proof. To further simplify the Hamiltonian, we introduce the Dirichlet-Neumann operator, denoted by $G[\zeta, h]$, which is defined in the standard manner (see also [23]):

$$
(2.14) \qquad G[\zeta, h]\varphi = \nabla\phi \cdot \mathbf{n}\sqrt{1+\zeta_x^2} = \phi_y - \zeta_x\phi_x.
$$

The dependence of the operator on ζ and h is suppressed hereafter for ease of notations. It can be expanded as a recursive convergent series $G = \sum_{j=0}^{\infty} G_j$ if the C^1-norm of η is smaller than some constant [5], and the first two terms read

$$
(2.15) \qquad G_0 = (-\partial_{xx})^{1/2} \tanh\left(h(-\partial_{xx})^{1/2}\right), \qquad G_1 = -\partial_x\zeta\partial_x - G_0\zeta G_0.
$$

Thus, based on the Dirichlet-Neumann operator, the Hamiltonian (2.9) can be rewritten as

$$
(2.16) \qquad \mathbb{H}[\zeta, \varphi] = \frac{1}{2}\int_{\mathbb{R}} \left[\varphi G\varphi + g\zeta^2 - \frac{\epsilon_0 V_0}{\rho} v_y\Big|_{y=-h} + \frac{2\sigma}{\rho}\left(\sqrt{1+\zeta_x^2} - 1\right)\right] \mathrm{d}x.
$$

For the deep-water case, the boundary condition (2.5) is usually replaced by $v \to E_0 y$ as $y \to -\infty$. We can define a new variable $w = v - E_0 y$ such that $\Delta w = 0$, $w_y \to 0$ as $y \to -\infty$, and $w(x, \zeta, t) = -E_0\zeta$. It then follows that the term associated with the electric field in the Hamiltonian (2.9) can also be expressed by using the Dirichlet-Neumann operator, specifically

$$
(2.17) \qquad \mathbb{H}[\zeta, \varphi] = \frac{1}{2}\int_{\mathbb{R}} \left[\varphi G\varphi + g\zeta^2 - \frac{\epsilon_0 E_0^2}{\rho}\zeta G\zeta + \frac{2\sigma}{\rho}\left(\sqrt{1+\zeta_x^2} - 1\right)\right] \mathrm{d}x.
$$

3. Asymptotic Models.

3.1. A shallow-water model. Nonlinear evolution equations can be derived in the long-wave limit. Here we present a procedure based on the Hamiltonian structure and analyticity property of the Dirichlet-Neumann operator, and interested readers may refer to [1, 3] for the

traditional derivation. It is first noticed that the Hamilton's equations (2.10) realize an extremum of the action $\int \mathbb{L} \, \mathrm{d}t$ with the Lagrangian

$$(3.1) \qquad \mathbb{L} = \int_{\mathbb{R}} \varphi \zeta_t \mathrm{d}x - \frac{1}{2} \int_{\mathbb{R}} \left[\varphi G \varphi + g\zeta^2 - \left. \frac{\epsilon_0 V_0}{\rho} v_y \right|_{y=-h} + \frac{2\sigma}{\rho} \left(\sqrt{1 + \zeta_x^2} - 1 \right) \right] \mathrm{d}x \,.$$

To proceed, we non-dimensionalize the problem by writing

$$(3.2) \qquad x = lX \,, \quad y = hY \,, \quad \zeta = h\Xi \,, \quad t = \frac{l}{c_0}T \,, \quad \varphi = c_0 l\Phi \,, \quad v = V_0 V$$

where l is the typical wavelength, and $c_0 = \sqrt{gh}$ is the long-wave speed. After changing variables, the rescaled Lagrangian $\mathbb{L}$, denoted by $\widetilde{\mathbb{L}}$, becomes

$$(3.3) \qquad \widetilde{\mathbb{L}} = \int_{\mathbb{R}} \left\{ \Phi \Xi_T - \frac{1}{2} \left[\frac{l}{\epsilon} \Phi \widetilde{G} \Phi + \Xi^2 - \left. \frac{\epsilon_0 V_0^2}{\rho g h^3} V_Y \right|_{Y=-1} + \frac{2\sigma}{\rho g h^2} \left(\sqrt{1 + \epsilon^2 \Xi_X^2} - 1 \right) \right] \right\} \mathrm{d}X \,,$$

where $\epsilon = \frac{h}{l}$ is a small parameter under the shallow-water approximation, and $\widetilde{G}$ is the rescaled Dirichlet-Neumann operator. Since

$$(3.4) \qquad \tanh\left(\epsilon \left(-\partial_{XX} \right)^{1/2} \right) = \epsilon \left(-\partial_{XX} \right)^{1/2} - \frac{\epsilon^3}{3} \left(-\partial_{XX} \right)^{3/2} + \cdots ,$$

the pseudo-differential operator $\widetilde{G}$ can be expanded, in terms of ϵ, as

$$(3.5) \qquad \widetilde{G} = -\frac{\epsilon}{l}\partial_{XX} - \frac{\epsilon}{l}\partial_X \Xi \partial_X - \frac{\epsilon^3}{3l}\partial_{XXXX} - \frac{\epsilon^3}{l}\partial_{XX}\Xi\partial_{XX} + \cdots .$$

The rescaled voltage potential satisfies $\epsilon^2 V_{XX} + V_{YY} = 0$ with the boundary conditions: $V = 0$ at $Y = \Xi$ and $V = -1$ at $Y = -1$. The asymptotic expansion of V can be written as $V = \overline{V}_0 + \epsilon^2 \overline{V}_1 + \epsilon^4 \overline{V}_2 + \cdots$. It then follows that, to leading order, $\overline{V}_0 = \frac{Y-\Xi}{1+\Xi}$. Substituting (3.5) and $\overline{V}_{0Y} = \frac{1}{1+\Xi}$ into the Lagrangian (3.3) and retaining the leading order terms, one obtains

$$(3.6) \qquad \overline{\mathbb{L}} = \int_{\mathbb{R}} \left[\Phi \Xi_T - \frac{1}{2}(1+\Xi)\Phi_X^2 - \frac{1}{2}\Xi^2 + \frac{E}{2}\frac{1}{1+\Xi} \right] \mathrm{d}X \,,$$

where $\overline{\mathbb{L}}$ is the truncated version of $\widetilde{\mathbb{L}}$ and $E = \frac{\epsilon_0 V_0^2}{\rho g h^3}$ is the electric Weber number. The inverse Weber number $\mathcal{W} = \frac{\sigma}{\rho g h^2}$ is supposed to be of $O(1)$ or smaller; thus, the rescaled force of surface tension becomes $O(\epsilon^2)$, which does not appear in the Lagrangian to leading order. Minimizing the approximate action $\int \overline{\mathbb{L}} \, \mathrm{d}t$ yields

$$(3.7) \qquad \begin{cases} S_T + (US)_X = 0 \,, \\ U_T + UU_X + S_X - E\dfrac{S_X}{S^3} = 0 \,, \end{cases}$$

where $U = \Phi_X$ and $S = 1 + \Xi$. The last two terms in the second equation of (3.7) represent the forces due to gravity and the electric field, respectively. System (3.7) can be rewritten in the matrix form as

$$(3.8) \qquad \begin{pmatrix} S \\ U \end{pmatrix}_T + \begin{pmatrix} U & S \\ 1 - \dfrac{E}{S^3} & U \end{pmatrix} \begin{pmatrix} S \\ U \end{pmatrix}_X = \begin{pmatrix} 0 \\ 0 \end{pmatrix} \,,$$

as derived in [3]. By the linear theory, it is readily shown that system (3.7) is unstable due to the destabilizing effect of the electric field when (3.8) is of elliptic type, i.e., the associated eigenvalues

are complex and can be written by $\lambda^{\pm} = U \pm \mathrm{i}\sqrt{\frac{E}{S^2} - S}$. To adapt the theory of shock formation for a 2×2 quasi-linear hyperbolic system pioneered by [14], a change of variables is required as first successfully used in [16] for studying a singularity problem in vortex sheets. It is also worth mentioning that these first-order systems have been further investigated by [4]. For the following initial conditions:

$$(3.9) \qquad S(X,0) = 1 + \delta \cos X, \quad U(X,0) = \delta \sin X,$$

we proceed by letting

$$(3.10) \qquad Z = \mathrm{i}X, \quad W(T,Z) = \mathrm{i}U(T,Z)$$

and then obtain

$$(3.11) \qquad \begin{pmatrix} S \\ W \end{pmatrix}_T + \begin{pmatrix} W & S \\ -1 + \frac{E}{S^3} & W \end{pmatrix} \begin{pmatrix} S \\ W \end{pmatrix}_Z = \begin{pmatrix} 0 \\ 0 \end{pmatrix}.$$

Then the initial conditions (3.9) are transformed into

$$(3.12) \qquad S(Z,0) = 1 + \delta \cosh Z, \quad U(Z,0) = \delta \sinh Z.$$

The eigenvalues of the system read

$$(3.13) \qquad \lambda^{\pm} = W \pm \sqrt{\frac{E}{S^2} - S},$$

and the corresponding left eigenvectors are

$$(3.14) \qquad \mathbf{e}^{\pm} = \left(\frac{\pm \sqrt{E - S^3}}{S^2}, 1 \right).$$

It is not difficult to find the Riemann invariants

$$(3.15) \qquad r = W + \int \frac{\sqrt{E - S^3}}{S^2} \, \mathrm{d}S, \quad s = W - \int \frac{\sqrt{E - S^3}}{S^2} \, \mathrm{d}S,$$

which are constant along the two characteristics $\mathrm{d}Z/\mathrm{d}T = \lambda^{\pm}$. Given an initial point Z_0, after similar calculations as [18], we can approximate the characteristics, up to $O(\delta^2)$, as follows:

$$(3.16) \qquad \begin{aligned} Z^+ &= Z_0 + \mu T + \delta e^{Z_0} f_1(T) + \delta e^{-Z_0} f_2(T) + O(\delta^2), \\ Z^- &= Z_0 - \mu T - \delta e^{Z_0} f_2(T) - \delta e^{-Z_0} f_1(T) + O(\delta^2), \end{aligned}$$

where $\mu = \sqrt{E - 1}$, and

$$(3.17) \qquad f_1(t) = \nu_1 T + \nu_2 e^{2\mu T}, \qquad f_2(t) = \nu_3 T + \nu_4 e^{-2\mu T}.$$

The parameter E is required to be greater than 1 such that $\mu \in \mathbb{R}$. The explicit expressions of the coefficients $(\nu_1, \nu_2, \nu_3, \nu_4)$ are tedious and unnecessary in estimating the leading order, so we omit the detail here. The formation of singularity causing an infinite slope in a finite time may occur in the following two scenarios.

- Two characteristics of Z^+ (or Z^-) cross each other. We must have

$$(3.18) \quad Z_0^{(1)} + \delta f_1(T) e^{Z_0^{(1)}} + \delta f_2(T) e^{-Z_0^{(1)}} = Z_0^{(2)} + \delta f_1(T) e^{Z_0^{(2)}} + \delta f_2(T) e^{-Z_0^{(2)}} + O(\delta^2)$$

for two distinct initial points, $Z_0^{(1)}$ and $Z_0^{(2)}$. We denote by T_c the minimal possible solution for the function $t(Z_0^{(1)}, Z_0^{(2)})$. It follows that $\frac{\partial t}{\partial Z_0^{(1)}} = \frac{\partial t}{\partial Z_0^{(2)}} = 0$ must be satisfied at $T = T_c$. It can then be readily shown that

$$(3.19) \quad e^{Z_0^{(1)}} = \frac{-1 + \sqrt{1 + 4\delta^2 f_1(T_c) f_2(T_c)}}{2\delta f_1(T_c)}, \quad e^{Z_0^{(2)}} = \frac{-1 - \sqrt{1 + 4\delta^2 f_1(T_c) f_2(T_c)}}{2\delta f_1(T_c)}.$$

By substituting (3.19) back into (3.16), an implicit equation for T_c in terms of δ is obtained:

$$(3.20) \qquad 2 + 2\ln\delta + \ln\left(-f_1\left(T_c\right)f_2\left(T_c\right)\right) = 0(\delta^2)\,.$$

It can be deduced from (3.20) that the asymptotic behavior of T_c when δ tends to zero is

$$(3.21) \qquad T_c \approx \frac{1}{\mu}\ln\frac{1}{\delta}\,.$$

- The envelope of the family of the characteristics Z^+ (or Z^-) reaches the real axis. The equation of the characteristics $\frac{\partial Z^+}{\partial Z_0} = 0$ admits identical solutions as (3.19) but at $T = T_d$. Substituting (3.19) into (3.16) and setting $Z^+ = 0$ yield

$$(3.22) \qquad 1 + \mu T_d + \ln\delta + \ln f_2(T_d) = 0(\delta^2)\,.$$

The asymptotic behavior of T_d at the leading order for small δ is identical to that of T_c, i.e.,

$$(3.23) \qquad T_d \approx \frac{1}{\mu}\ln\frac{1}{\delta}\,.$$

The theory developed in this section can be used to predict the critical time of singularity formation in the limit $\delta \to 0$. The infinity slope is believed to be related to the touch-down phenomenon where the fluid touches the lower boundary. In what follows, we will conduct fully nonlinear numerical computations to find the blowup times in the shallow-water case and compare them with the theoretical estimations.

3.2. A deep-water model. When the fluid depth is considerably large, the instability of the free surface still develops in the unstable regime, causing the formation of a different type of singularity. To understand the mechanism of such electricity-generated singularity, we focus on the particular case of strong electric fields such that the electric force is dominant over the gravity and capillary forces at a specific wavenumber provided $1/E_b \ll k \ll E_b$. Under such an assumption, the problem is reformulated in this section using the Dirichlet-Neumann operator to propose a model in the deep-water limit.

Following [13], we assume the electric force dominates over gravity and surface tension, thus the Lagrangian in the deep-water scenario reads

$$(3.24) \qquad \mathbb{L} = \int_{\mathbb{R}}\varphi\zeta_t\mathrm{d}x - \frac{1}{2}\int_{\mathbb{R}}\left(\varphi G\varphi - \frac{\epsilon_0 E_0^2}{\rho}\zeta G\zeta\right)\mathrm{d}x\,.$$

The pseudo-differential operator can be expanded as

$$(3.25) \qquad G = -\mathcal{H}\partial_x - \partial_x\zeta\partial_x - \mathcal{H}\partial_x\zeta\mathcal{H}\partial_x + \cdots\,.$$

Here $\mathcal{H}$ is the Hilbert transform with the Fourier symbol $\mathrm{i}\,\mathrm{sgn}(k)$, and it can also be defined in the physical space as

$$(3.26) \qquad \mathcal{H}[f](x) = \frac{1}{\pi}\,\mathrm{P.V.}\int_{-\infty}^{\infty}\frac{f(x')}{x' - x}dx'\,,$$

where 'P.V.' denotes the Cauchy principal value of the integral. We retain the Dirichlet-Neumann operator expansion valid up to the second order of ζ and substitute it into the Lagrangian. After minimizing the truncated action by taking the variational derivatives with respect to φ and ζ, one obtains
(3.27)
$$\begin{cases} \zeta_t + \mathcal{H}\partial_x\varphi = -\partial_x(\zeta\partial_x\varphi) - \mathcal{H}\partial_x(\zeta\mathcal{H}\partial_x\varphi)\,, \\ \varphi_t + \frac{\epsilon_0 E_0^2}{\rho}\mathcal{H}\partial_x\zeta = \frac{1}{2}\left[(\mathcal{H}\partial_x\varphi)^2 - \varphi_x^2\right] - \frac{\epsilon_0 E_0^2}{2\rho}\left[(\mathcal{H}\partial_x\zeta)^2 - \zeta_x^2\right] - \frac{\epsilon_0 E_0^2}{\rho}\left[\partial_x(\zeta\partial_x\zeta) + \mathcal{H}\partial_x(\zeta\mathcal{H}\partial_x\zeta)\right]\,. \end{cases}$$

It is noted that system (3.27) can also be derived by directly expanding the Dirichlet-Neumann operator in the kinematic and dynamic boundary conditions. The linear part of system (3.27) can be recast to

$$(3.28) \qquad\qquad P_t + A_0\, \mathcal{H}\partial_x P = 0\,,$$

$$(3.29) \qquad\qquad Q_t - A_0\, \mathcal{H}\partial_x Q = 0\,,$$

with

$$(3.30) \qquad\qquad P = \frac{1}{2}\left(\varphi + A_0\zeta\right),\qquad Q = \frac{1}{2}\left(\varphi - A_0\zeta\right),$$

where we denote $A_0 = \sqrt{\frac{\epsilon_0 E_0^2}{\rho}}$ for ease of notations. As remarked in [13], equation (3.28) characterizes the growth of the variables, whereas (3.29) is concerned with attenuation, which is much less important in studying instability. It is reasonable to make a further assumption that Q is identically zero up to $O(\zeta^2)$ such that all the nonlinear terms in Q are eliminated. It follows that $\varphi = A_0\zeta$ up to the quadratic order, and (3.27) reduces to

$$(3.31) \qquad\qquad P_t + A_0\, \mathcal{H}\partial_x P = -2\left(PP_x + \mathcal{H}P\mathcal{H}P_x\right)_x\,,$$

We note that (3.31) is equivalent to the system derived in [13] by considering interfacial waves between two semi-infinite dielectric fluids. Using the formula associated with the Hilbert transform $\mathcal{H}[fg] = f\mathcal{H}g + g\mathcal{H}f + \mathcal{H}[\mathcal{H}f \cdot \mathcal{H}g]$, we can recast equation (3.31) to

$$(3.32) \qquad\qquad F_t + \mathrm{i}A_0 F_x = -(1 - \mathrm{i}\mathcal{H})(FF_x^*)_x\,.$$

where $F = (1 - \mathrm{i}\mathcal{H})P$ and the superscript asterisk represents complex conjugation. Furthermore, (3.32) can be solved using a complex variable method in which $F(x,t)$ can be expressed by a sum of simple poles in the complex plane, as shown by [13]. If we pick $F(x,0) = \frac{\mathrm{i}S/2}{x + \mathrm{i}a_0}$ as the initial condition, where S and a_0 are real constants, the solution reads $F(x,t) = \frac{\mathrm{i}S/2}{x + \mathrm{i}a(t)}$, and $a(t)$ satisfies

$$(3.33) \qquad\qquad \frac{\mathrm{d}a}{\mathrm{d}t} = -A_0 + \frac{S}{4a^2}\,,\qquad a(0) = a_0\,.$$

We remark that equation (3.33) was obtained by noticing

$$\mathcal{H}\left[\frac{1}{x - \mathrm{i}a}\right] = \frac{-\mathrm{i}}{x - \mathrm{i}a}\,,\quad \mathcal{H}\left[\frac{1}{x + \mathrm{i}a}\right] = \frac{\mathrm{i}}{x + \mathrm{i}a}\,,\quad \text{and}\ \mathcal{H}\left[\frac{1}{(x - \mathrm{i}a)^2}\right] = \frac{-\mathrm{i}}{(x - \mathrm{i}a)^2}\,.$$

If S is negative, integrating equation (3.33) yields

$$(3.34) \qquad\qquad \frac{a}{A_0} - \frac{1}{2A_0}\sqrt{\frac{|S|}{A_0}}\arctan\left(2a\sqrt{\frac{A_0}{|S|}}\right) = t_c - t\,,$$

where the integration constant t_c reads

$$(3.35) \qquad\qquad t_c = \frac{a_0}{A_0} - \frac{1}{2A_0}\sqrt{\frac{|S|}{A_0}}\arctan\left(2a_0\sqrt{\frac{A_0}{|S|}}\right).$$

Upon noticing the specific expression of the solution $F(x,t)$, the amplitude of the free surface approaches infinity at $x = 0$, as $t \to t_c$. However, we should emphasize that the above argument only provides a possibility for singularity formation, and the effectiveness of this theoretical prediction is ambiguous. That is because the expansion of the Dirichlet-Neumann operator does not converge when the wave amplitude is sufficiently large. The above discussion indicates that reduced models are sometimes limited, and it is vital to understand their respective applicable scopes.

In contrast to the infinite-amplitude singularity predicted by the weakly nonlinear theory, Zubarev showed in [26] that the free surface develops a cusp singularity with the slope and curvature becoming infinite in a finite time in the full Euler problem in deep water where the electric field provides the only restoring force. More precisely, the spatial behaviour of the solution close to the singular point $x = x_k$ features, to leading order,

$$(3.36) \qquad \zeta(x) - \zeta(x_k) = O\left(|x - x_k|^{2/3}\right).$$

The above estimate was obtained in [26], with the aid of the well-known Laplacian growth equations, for a particular case where the singularity is formed at the trough of the free surface, i.e., the cusp is perpendicular to the $x-$axis. More generally, the cusp formation can occur at any position along the interface with a qualitatively similar asymptotic spatial behaviour to (3.36). It is usually referred to as the 2/3 power cusp in the literature, which was intensively investigated in other contexts of fluid dynamics, e.g., see [20] for Stefan problems and [11] for Hele-Shaw flows. In our situation, such a result predicts that the fluid system in deep water is destabilized, and the free surface exhibits the formation of 2/3 power cusps in the presence of very strong electric fields, which will be helpful in examining the fully nonlinear computations of the Euler equations.

4. Numerical Scheme. We describe the numerical scheme for the electrified Euler equations in this section. We first non-dimensionalize the system by choosing

$$(4.1) \qquad \left[\frac{\sigma}{\rho g}\right]^{1/2}, \qquad \left[\frac{\sigma}{\rho g^3}\right]^{1/4}, \qquad \left[\frac{\sigma^3}{\rho^3 g}\right]^{1/4}, \qquad \frac{V_0}{h}\left[\frac{\sigma}{\rho g}\right]^{1/2}$$

as the reference length, time, velocity potential, and voltage potential, respectively. Under this scaling, the bottom boundary is given by $y = -H$, where the rescaled depth $H = h\sqrt{\rho g/\sigma}$. The governing equations (2.1) and (2.2) remain the same, while the dynamic boundary condition (2.7) becomes

$$(4.2) \qquad \phi_t + \frac{1}{2}|\nabla\phi|^2 + \zeta + \frac{E_b}{2}|\nabla v|^2 - \frac{\zeta_{xx}}{(1+\zeta_x^2)^{3/2}} = 0, \qquad \text{on} \quad y = \zeta(x,t),$$

where $E_b = \frac{\epsilon_0 V_0^2}{h^2\sqrt{\rho g \sigma}}$. The boundary conditions for the voltage potential are now scaled to be

$$(4.3) \qquad v = -H, \qquad\qquad\qquad \text{on } y = -H,$$
$$(4.4) \qquad v = 0, \qquad\qquad\qquad \text{on } y = \zeta(x,t).$$

The kinematic boundary conditions (2.3) and (2.6) remain unchanged. By following [7] to linearize the governing equations, it is not difficult to obtain the dispersion relation

$$(4.5) \qquad c_p^2 = \left(\frac{1}{k} + k\right)\tanh(kH) - E_b,$$

where k is the wavenumber and c_p is the phase speed. The fluid system is destabilized for a given E_b at a particular value of k when the right-hand side of (4.5) is negative at this wavenumber. In what follows, we will show that the destabilization always occurs at some wavenumber for $E_b = 2.5$. An example for $H = 5$ is presented in Figure 4.1.

A numerical method pioneered by [6], based on a conformal mapping technique, is used for fully nonlinear time-dependent computations. The fluid domain is transformed onto a strip with depth D in the new $\xi - \eta$ plane. The harmonic conjugate of $x(\xi, \eta)$ can be obtained via the Cauchy-Riemann equations for the analytic function $z(\xi, \eta) = x(\xi, \eta) + iy(\xi, \eta)$. Similarly, we can derive the harmonic conjugates of $\phi(\xi, \eta)$ and $v(\xi, \eta)$, denoted by $\psi(\xi, \eta)$ and $\nu(\xi, \eta)$. We write the surface variables in the transformed plane as $X(\xi, t) \equiv x(\xi, 0, t)$, $Y(\xi, t) \equiv y(\xi, 0, t)$, $\Phi(\xi, t) \equiv \phi(\xi, 0, t)$, $\Psi(\xi, t) \equiv \psi(\xi, 0, t)$, $V(\xi, t) \equiv v(\xi, 0, t)$, and $\Theta(\xi, t) \equiv \nu(\xi, 0, t)$. The map can be formally defined as the solutions to the following boundary value problems

$$(4.6) \qquad y_{\xi\xi} + y_{\eta\eta} = 0, \qquad \psi_{\xi\xi} + \psi_{\eta\eta} = 0, \qquad v_{\xi\xi} + v_{\eta\eta} = 0, \qquad\qquad \text{for} \quad -D < \eta < 0,$$
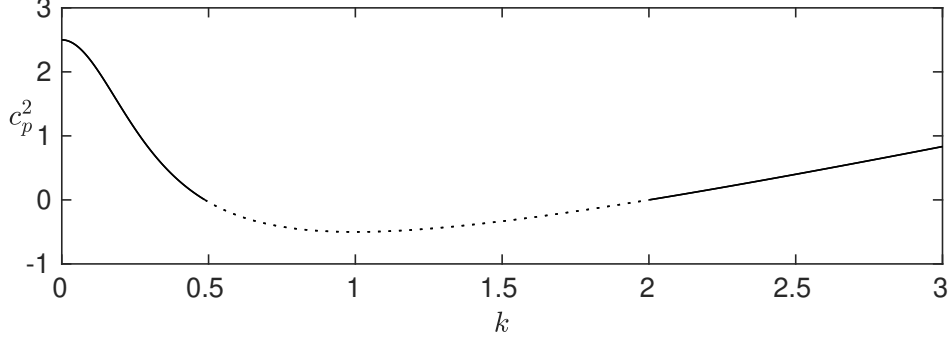
FIG. 4.1. *Linear dispersion relation for $H = 5$ and $E_b = 2.5$. The solid curves are for $c_p^2 > 0$, and the dotted curve is in the area of destabilization.*

$$
\begin{aligned}
(4.7) \quad & y = Y(\xi, t), & \psi = \Psi(\xi, t), & \quad v = V(\xi, t) = 0, & \text{on} \quad \eta = 0, \\
(4.8) \quad & y = -H, & \psi = Q, & \quad v = -H, & \text{on} \quad \eta = -D,
\end{aligned}
$$

where $Y(\xi, t) = \zeta(\xi, 0, t)$, and Q is a constant. We choose $Q = \langle \Psi \rangle$, with $\langle \cdot \rangle$ the mean value defined as

$$
(4.9) \qquad \langle f \rangle = \frac{1}{L} \int_{-L/2}^{L/2} f(\xi) \, \mathrm{d}\xi,
$$

where $\left[-\frac{L}{2}, \frac{L}{2} \right]$ is the computational domain, and L is usually set to be the wavelength. Following [7], it can be shown that

$$
(4.10) \qquad D = H + \langle Y \rangle, \quad X_\xi = 1 - \mathcal{T}[Y_\xi], \quad \Phi_\xi = -\mathcal{T}[\Psi_\xi], \quad \Theta_\xi = -\frac{H}{D} + \mathcal{T}[V_\xi],
$$

where $\mathcal{T}[\cdot]$ is defined by

$$
(4.11) \qquad \mathcal{T}[f](\xi) = \frac{1}{2D} \, \mathrm{P.V.} \int f(\xi') \coth\left(\frac{\pi}{2D}(\xi' - \xi) \right) \mathrm{d}\xi'.
$$

We note that $V_\xi = 0$ as v is identically zero everywhere on the free surface. Again, we follow [7] to derive the evolution equations, yielding

$$
(4.12) \qquad Y_t = Y_\xi \mathcal{T}\left[\frac{\Psi_\xi}{J} \right] - X_\xi \frac{\Psi_\xi}{J},
$$

$$
(4.13) \qquad \Phi_t = \frac{1}{2J}\left(\Psi_\xi^2 - \Phi_\xi^2 \right) - Y - \frac{E_b H^2}{2D^2 J} + \frac{X_\xi Y_{\xi\xi} - Y_\xi X_{\xi\xi}}{J^{3/2}} + \Phi_\xi \mathcal{T}\left[\frac{\Psi_\xi}{J} \right],
$$

where $J = X_\xi^2 + Y_\xi^2$ is the Jacobian of the conformal map. The $\mathcal{T}$-transform can be computed numerically using its Fourier symbol as follows

$$
(4.14) \qquad \mathcal{T}[f] = \mathcal{F}^{-1}\left[\mathrm{i} \coth(kD) \mathcal{F}[f] \right],
$$

where $\mathcal{F}$ is the Fourier transform. The wave height and the distance from the bottom are written respectively as

$$
(4.15) \qquad A = \left| \min_{\xi \in \mathbb{R}} Y \right|, \qquad d = H - A.
$$

A fourth-order Runge-Kutta method is used for time-stepping with 2^{10} to 2^{14} grid points and the time step of 10^{-4} to 10^{-9} to solve (4.12)–(4.13).
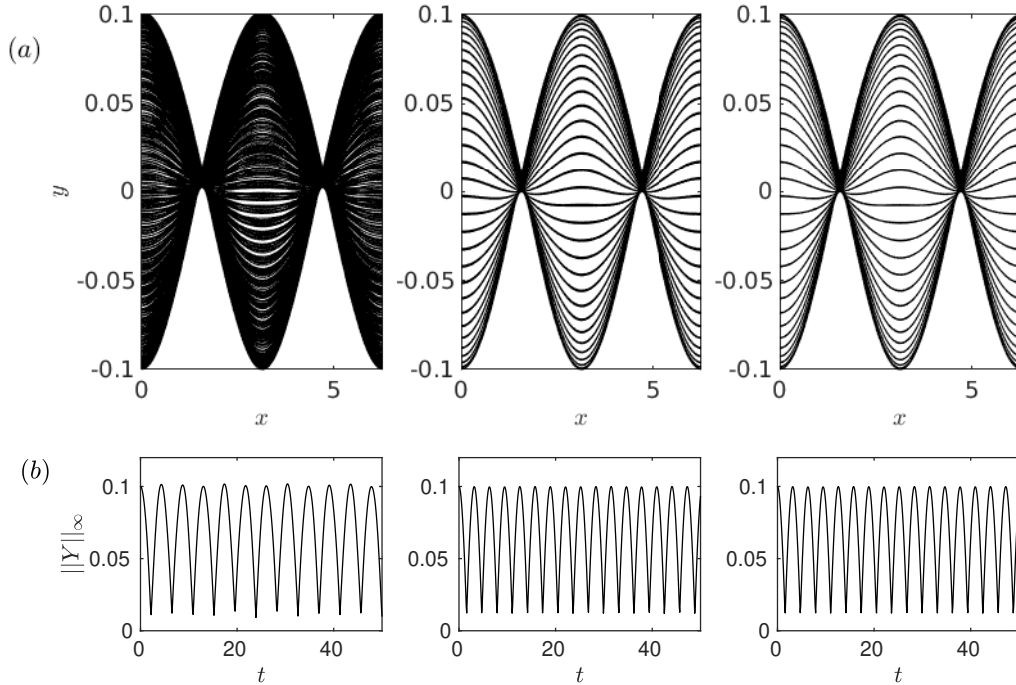
FIG. 5.1. *(a) Surface evolution in the stable regime for $E_b = 1$ and $H = 1$, 20, and 500 (from left to right). (b) The maximal values of $|Y|$ as time evolves ($t \in [0, 50]$).*

5. Numerical Results.

5.1. Stable regime. We start by examining the numerical scheme in the stable regime for $E_b = 1$, with the grid number $N = 2^{10}$ and time step $dt = 10^{-4}$. The initial uniform solution on the domain $[0, 2\pi]$ is perturbed by a small spatially periodic disturbance, specifically $Y = 0.1 \cos \xi$. The time evolution of the surface is presented in Figure 5.1 for $t \in [0, 50]$ with $H = 1$, 20, and 500. We observe standing waves with quasi-periodic oscillations akin to those obtained in [2] by solving a long-wave evolution system. Such oscillatory behaviour will continue for an infinite time. The frequency of oscillation in the dynamics is larger as the depth becomes deeper, as shown in Figure 5.1(b). In other words, there are more numerical observations for smaller H while computing with the same time step in a fixed time interval as confirmed from Figure 5.1(a).

5.2. Unstable regime. In the remaining part of the work, we confine our attention to the unstable regime in which the linear phase speed from (4.5) no longer admits a real solution for some wavenumber, causing the fluid system to be destabilized. For an in-depth understanding of singularity formation, we investigate the dynamics of a monochromatic periodic wave under the effect of a strong electric field in an unstable regime for liquids of various depths.

5.2.1. Destabilization of a periodic wave on shallow water. For the problem in the shallow-water regime, similar to [2], the fluid surface has a very localized structure when the trough approaches and eventually touches the solid bottom. We refer to this phenomenon as touch-down singularity hereafter. The parameters are chosen to be $H = 0.1$ and $E_b = 2.5$, corresponding to the unstable regime of destabilization. The initial condition for the system is $Y = \epsilon \cos \xi$ for $\epsilon = 0.001, 0.002, \cdots, 0.01$ with $N = 2^{13}$ collocation points and $dt = 10^{-7}$ for time integration. The snapshots of wave profiles obtained in the experiment for $\epsilon = 0.01$ are shown in Figure 5.2, where the touch-down singularity is observed.

Meanwhile, we record the critical times when the distance between the bottom boundary and the lowest point of the free surface is less than 0.002. It is not difficult to compare these values to the asymptotic predictions of the formation of infinite slope from (3.21) and (3.23) with a simple
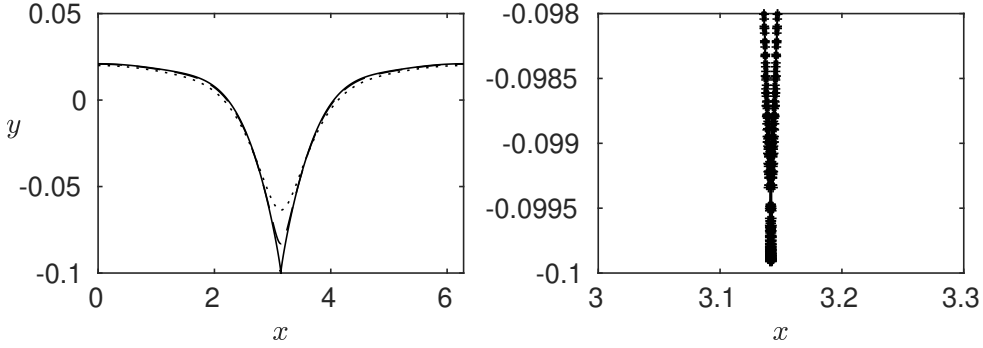
FIG. 5.2. *(Left) Snapshots of wave profiles in the numerical experiment of destabilization on a shallow fluid with $H = 0.1$ and $E_b = 2.5$ at $t = 1.1$ (dotted curve), $t = 1.14$ (dashed curve), and $t = 1.14832$ (solid curve). (Right) A blow-up graph of the wave profile at $t = 1.14832$.*
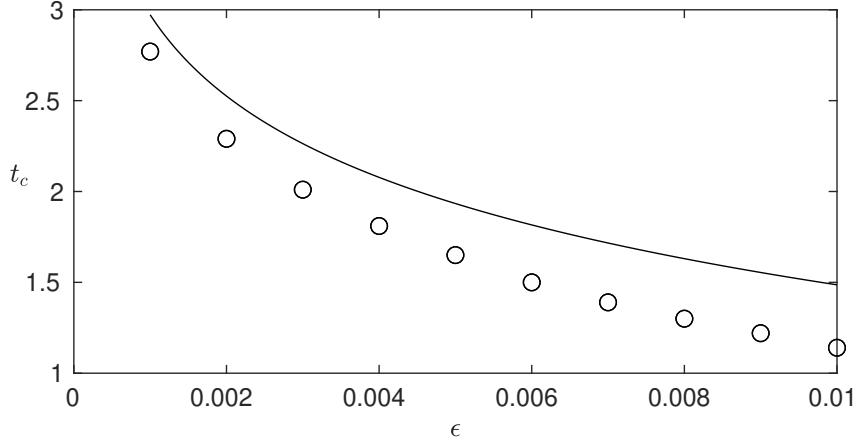

FIG. 5.3. *Comparison of the critical times (denoted by t_c) for the free surface almost touching the bottom between the full Euler computations (black dots) and the asymptotic predictions (black curve) of formation of infinity slope for different values of ϵ.*

change of scaling. Numerical results of the full Euler equations and theoretical predictions are plotted in Figure 5.3, where a good agreement has been found. It is a piece of strong numerical evidence that these two times, the touch-down time observed in the numerical computations and the time for forming an infinite slope predicted by the asymptotic theory, are identical. However, the scaling used in the asymptotic theory is inappropriate near singularity formation since the capillary force also tends to infinity and cannot be ignored. Because the surface curvature has a faster divergence rate to infinity than the slope, the asymptotic theory, which has not taken the surface tension effect into account, always slightly overestimates the blowup time (see Figure 5.3).

To further understand such touch-down singularity, we follow [3] to seek a self-similar solution when the free surface reaches the bottom at $t = t_s$ and $x = x_s$ by defining

$$(5.1) \qquad \qquad \tau = t_s - t \ll 1 \,, \quad \chi = \frac{x - x_s}{\tau^b} = O(1)$$

and writing

$$(5.2) \qquad \qquad d = \tau^a p(\chi) \,, \quad \phi_x = \tau^{b-1} q(\chi) \,,$$

where (2.3) has been used to derive the asymptotics of ϕ_x. Since the gravity term remains finite at $t = t_s$, the dynamic boundary condition (2.7) is satisfied by balancing to leading order,
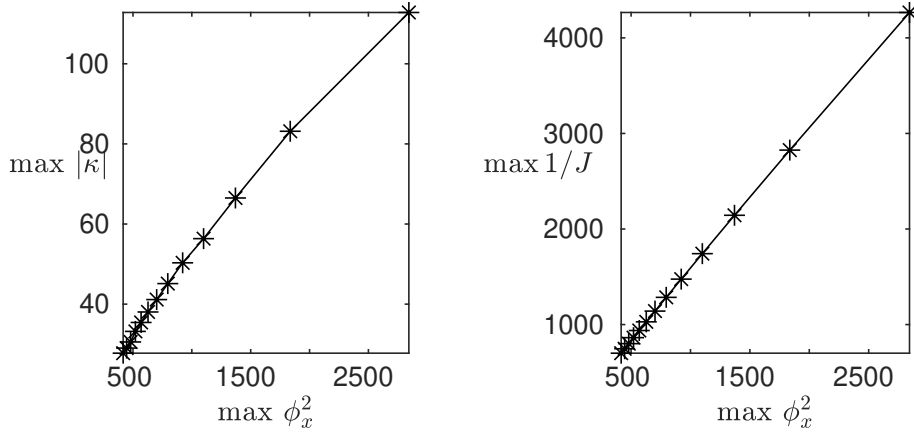
FIG. 5.4. *Maximal values of $|\kappa|$ and $1/J$ versus the maximal value of ϕ_x when t is close to t_s ($t \in [1.148, 1.14832]$).*

- the surface tension, κ, of order $O(\tau^{b-2a})$,
- the electric force, ζ_x^2, of order $O(\tau^{2a-2b})$,
- terms associated with the velocity potential, $\phi_t + \frac{1}{2}\phi_x^2$, of order $O(\tau^{2b-2})$.

A simple calculation shows that these terms may be balanced and all retained in the equation when $b = 0.8$ and $a = 0.6$. The parameter values are found to be different from the ones obtained in [3], where the electric force was ignored at the touch-up while forming the self-similar solutions due to the physical configuration. We compare the maximal value of κ (surface tension) and $1/J$ (electric force) to that of ϕ_x^2 when t is close to t_s. The quantities are found to be linearly dependent, as shown in Figure 5.4. Hence, the scaling being used is consistent.

The exact touch-down time can be estimated by a quick and efficient approach of the least squares method. We conduct computations for d and ϕ_x^2 and obtain the same estimator for t_s, which is found to be $t_s \approx 1.148326$. The data fittings are presented in Figure 5.5, where an excellent agreement has been found between the simulation data and the least squares estimators. By writing

$$(5.3) \qquad p(\chi) \sim |\chi|^{n_p}, \quad q(\chi) \sim |\chi|^{n_q},$$

after similar calculations to those in [2], it is obtained for $\chi \gg 1$ that $n_p = \frac{3}{4}$ and $n_q = -\frac{1}{4}$, leading to

$$(5.4) \qquad d \sim |x - x_s|^{\frac{3}{4}}, \quad \phi_x \sim |x - x_s|^{-\frac{1}{4}}.$$

The maximal gradient and curvature of the free surface both tend to infinity when the touch-down occurs. Hence, a cusp is expected to be formed. This is confirmed by the numerical simulation, as seen from the solid curve in Figure 5.2. In summary, the destabilization of electrocapillary-gravity waves on shallow water leads to the formation of a cusp that touches down the bottom boundary, causing a rupture.

5.2.2. Destabilization of a periodic wave on deep water. It is evident that the touch-down singularity no longer occurs in the case of deep water; instead, we can observe the pinch-off phenomenon in numerical experiments. More specifically, the instability due to the electric destabilization still develops in the unstable regime and causes a growth in the surface displacement, which surges up to its maximum amplitude, evolves into a mushroom-shaped structure, and ends up with two closed bubbles due to the presence of surface tension. The feature is confirmed by the direct numerical computations of the electrified Euler equations. We stop the numerical computation when the self-intersecting structure appears since further interface evolution shows multiple self-intersecting points leading to a non-physical solution. A typical example for $H = 20$
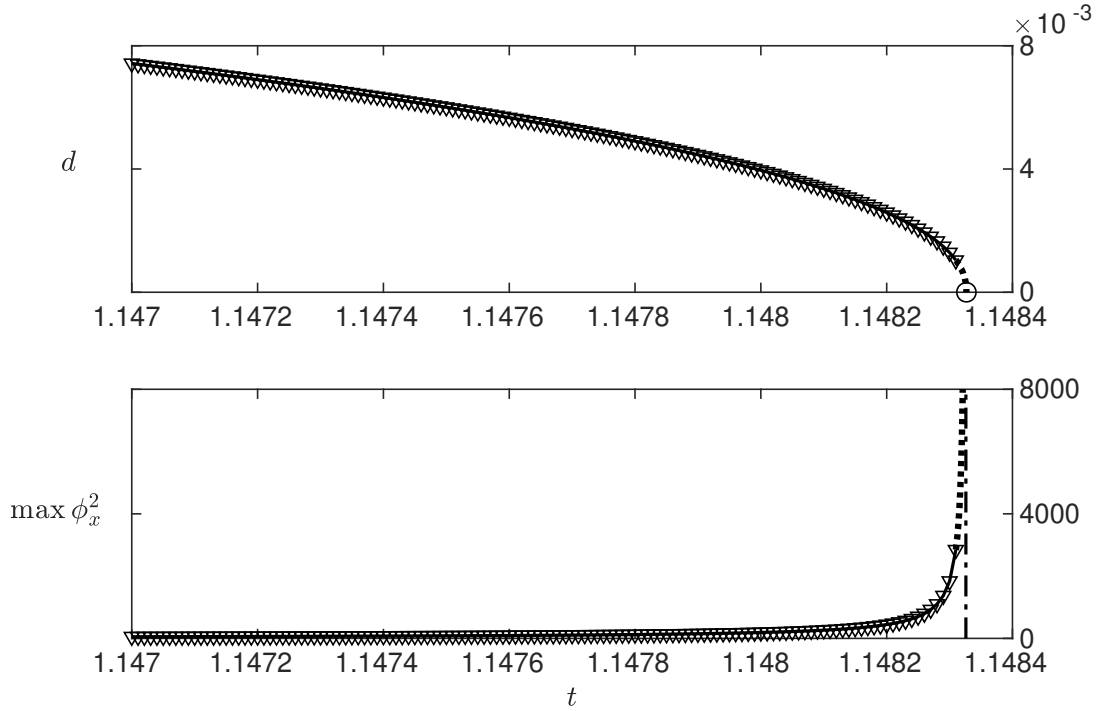
FIG. 5.5. *Upper: time evolution of d near the touch-down singularity with $H = 0.1$ and $E_b = 2.5$. The triangles are the data obtained from the numerical simulations. The solid curve is the fitted curve, and the dotted curve is the prediction of the self-similar solution. The circle point is the intersection of the dotted curve and the horizontal axis. (Lower) time evolution of $\max \phi_x^2$ near the touch-down singularity.*
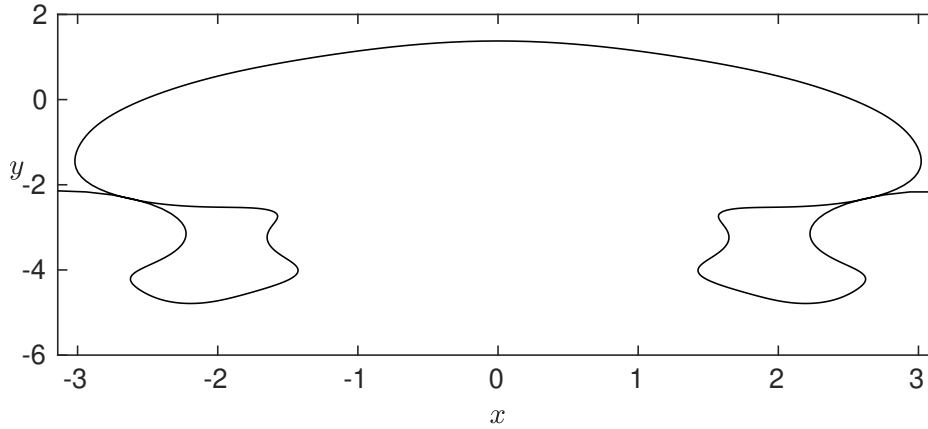

FIG. 5.6. *Snapshot of the wave profile at $t = 8.25$ in the numerical experiment of destabilization with $H = 20$ and $E_b = 2.5$.*

and $E_b = 2.5$ is presented in Figure 5.6. Qualitatively similar results are obtained for more considerable depths. Hence, the numerical result indicates that the formation of bubbles, a physical constraint, occurs earlier than the generation of the touch-down or cusp singularities caused by the electric field.

Next, we focus on the case where the fluid depth is deep enough to avoid touch-down but insufficient to allow pinch off. Under such circumstances, the effect of the electric field plays a dominant role in the singularity formation. To this end, the water depth must be chosen carefully
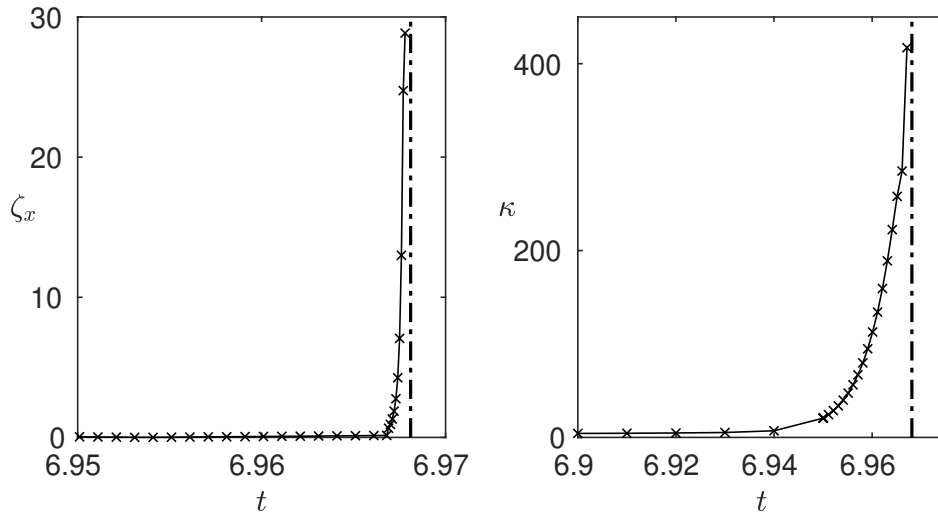
FIG. 5.7. *Left: time evolution of the maximal surface slope for $H = 5$ and $E_b = 2.5$. Right: time evolution of the maximal surface curvature for $H = 5$ and $E_b = 2.5$. The dash-dotted curves are the asymptotes estimated by the least square method.*

for the numerical study to guarantee that neither touch-down nor pinch-off occurs. In practice, we select $H = 5$ for simulations, so the deep-water approximations are still appropriate. The wave magnitude increases in the same manner as in the deep-water case until the wave trough is not far from the bottom boundary. Accordingly, as seen from the right panel of Figure 5.7, the maximal surface curvature dramatically surges and tends to infinity at a critical time. The maximal slope is also examined and sketched in the left panel of Figure 5.7. It also tends to infinity but is much slower in comparison to the growth rate of the curvature. The wave profile before the collapse of the numerical experiment is presented in Figure 5.7. Suspicious singular behaviours have been observed at several positions on the free surface. The 2/3 power asymptotics are fitted to a point (x_k, y_k) with the most significant feature (extreme curvature) and sketched in the right panel of Figure 5.7, in which a good agreement has been found. The full examination of the cuspidal curve is achieved by evaluating the following quantities near the singular point

$$(5.5) \qquad M_1 = \frac{\alpha_1^2}{\alpha_2^3}, \qquad M_2 = \frac{\alpha_1^2}{\alpha_2^2}, \qquad M_3 = \frac{\alpha_1}{\alpha_2^3},$$

where α_1 and α_2 are the distances defined in Figure 5.8. It follows that M_1 remains finite, M_2 tends to zero, and M_3 tends to infinity on the occasion of singularity formation. Such a theoretical prediction is confirmed by the simulation results listed in Table 5.1 and presented in Figure 5.10, which shows strong numerical evidence that the cusp follows 2/3 power asymptotics. The liquid surface around $x = x_k$ tends to have infinite curvature that causes a breakdown of the wave structure. The least-square estimator returns $t_k = 6.9795$ for the present example, also shown in Figure 5.9. As previously investigated, we believe the cusp formation causes this curvature singularity in deep water. It is developed at multiple positions on the free surface, unlike the touch-down singularity in shallow water, where the cusp is always formed at the lowest point of the free surface.

6. Conclusion. The transition of the singularities arising in electrocapillary-gravity waves on a dielectric fluid of finite depth under vertical electric fields has been investigated. Unsteady numerical simulations have been performed based on a time-dependent conformal mapping technique. The shallow-water, deep-water, and medium-depth cases were all studied. When the water depth is shallow, the surface touches down the bottom boundary, causing the surface slope and curvature to tend to infinity, forming a cusp at a terminal finite time. The surface displacement
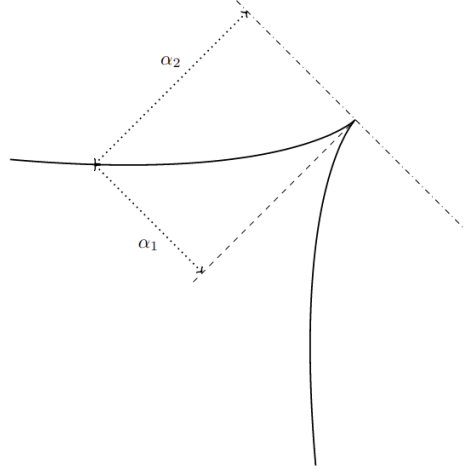
FIG. 5.8. *Schematic of a cuspidal curve (solid), the symmetry axis of the cusp (dashed)and its perpendicular passing through the cusp (dashed-dotted). The plot-scale is exaggerated for illustrating purpose.*
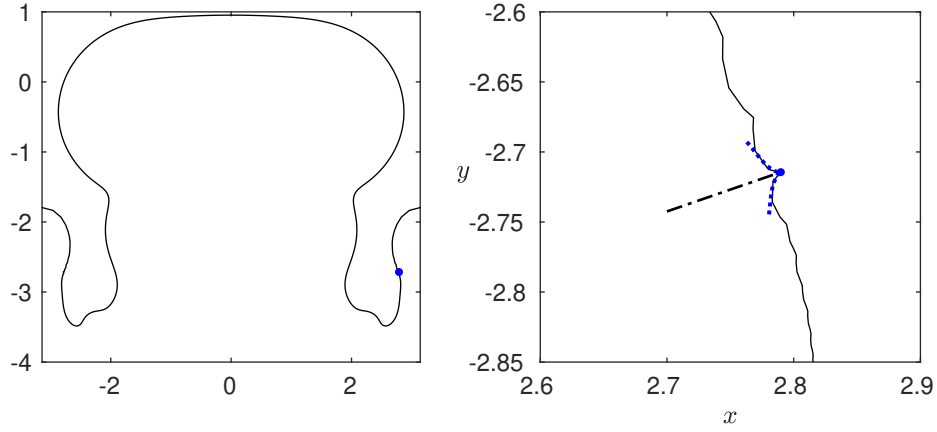

FIG. 5.9. *Left: snapshot of the wave profile at $t = 6.9665$, close to the cusp blow-up time. Right: The blow-up graph near the dot highlighted in the left panel. The 2/3 power asymptotic behaviours are fitted and depicted in dotted curves. The line of symmetry is sketched in a dotted-dashed curve.*

Evaluation of (5.5) at P_1	M_1	M_2	M_3
$t = 6.9663$	44.1786	0.3646	8.8636×10^3
$t = 6.9664$	45.0139	0.3624	9.2894×10^3
$t = 6.9665$	44.6226	0.3522	9.5259×10^3
Evaluation of (5.5) at P_2	M_1	M_2	M_3
$t = 6.9663$	44.0283	0.4230	7.0459×10^3
$t = 6.9664$	34.5310	0.3035	7.1312×10^3
$t = 6.9665$	28.6152	0.2205	7.9076×10^3

TABLE 5.1

The quantities given in (5.5) at the nearest neighbours (P_1 and P_2) of the singular point before the numerical simulation is ended due to a blow-up in the surface curvature.
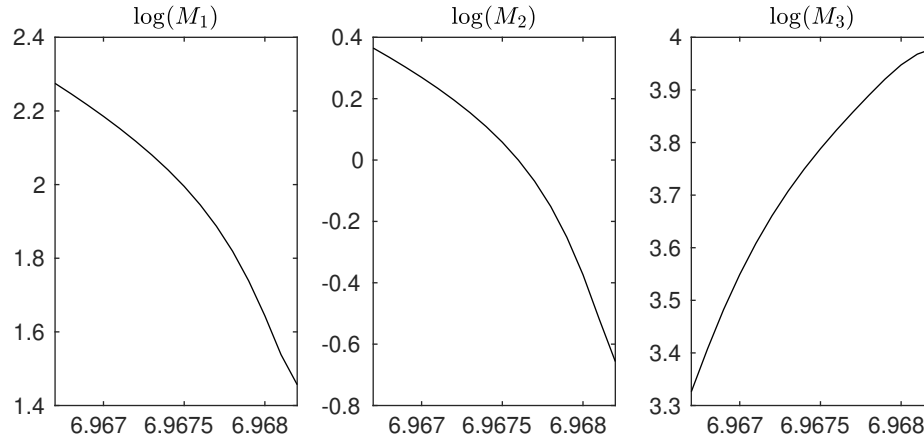
FIG. 5.10. *The behaviours of M_1, M_2, and M_3 in the logarithm scale versus time at the neighbour point P_2 near the singularity before the blow-up of the surface curvature.*

increases when the water depth is deep, forming self-intersecting structures and trapped bubbles before touch-down/cusp/curvature singularities appear. When the water depth is deep but insufficient for bubble formation, the maximal surface curvature and the surface slope grow and eventually tend to infinity, causing the surface structure to collapse. Motivated by theoretical results for the deep-water case in the absence of gravity and surface tension (electric field only), the 2/3 power cuspidal singularity is confirmed on a dielectric fluid of medium depth, though the singular points do not occur in the middle.

REFERENCES

[1] L. L. Barannyk and D. T. Papageorgiou, Fully nonlinear gravity-capillary solitary waves in a two-fluid system of finite depth, *J. Eng. Math.* **42**, 321–339 (2002).

[2] L. L. Barannyk, D. T. Papageorgiou, P. G. Petropoulos, and J.-M. Vanden-Broeck, Nonlinear dynamics and wall touch-up in unstably stratified multilayer flows in horizontal channels under the action of electric fields, *SIAM J. Appl. Math.* **75**(1), 92–113 (2015).

[3] H. Broadley and D. T. Papageorgiou, Nonlinear gravity electro-capillary waves in two-fluid system: Solitary and periodic waves and their stability, *J. Eng. Math.* **133**, 6 (2022).

[4] R. E. Caflisch, N. Ercolani, T. Y. Hou, and Y. Landis, Multi-valued solutions and branch point singularities for nonlinear hyperbolic or elliptic systems, *Comm. Pure Appl. Math.* **46**(4), 453–499 (1993).

[5] W. Craig and C. Sulem, Numerical simulation of gravity waves. *J. Comput. Phys.* **108**, 73–83 (1993).

[6] A. I. Dyachenko, V. E. Zakharov, and E. A. Kuznetsov, Nonlinear dynamics of the free surface of an ideal fluid, *Plasma Phys. Rep.* **22**(10), 829–840 (1996).

[7] T. Gao, A. Doak, J.-M. Vanden-Broeck, and Z. Wang, Capillary-gravity waves on a dielectric fluid of finite depth under normal electric field, *Eur. J. Mech. B/Fluid* **77**, 98-107 (2018).

[8] T. Gao, P. A. Milewski, D. T. Papageorgiou, and J.-M. Vanden-Broeck, Dynamics of fully nonlinear capillary-gravity solitary waves under normal electric fields, *J. Eng. Math.* **108**(1), 107–122 (2018).

[9] T. Gao, Z. Wang, and J.-M. Vanden-Broeck, Nonlinear wave interactions on the surface of a conducting fluid under vertical electric fields, *Phys. D* **446**, 133651 (2023).

[10] E. M. Griffing, S. G. Bankoff, and M. J. Miksis, Electrohydrodynamics of thin flowing films, *J. Fluids Eng.* **128**(2), 276–283 (2006).

[11] S. D. Howison, Cusp development in Hele–Shaw flow with a free surface. *SIAM J. Appl. Math.* **46**(1), 20-26 (1986).

[12] S. F. Kistler and P. M. Schweizer, Liquid film coating: scientific principles and their technological implications, 401–536, Chapman & Hall (1997).

[13] E. A. Kochurin, N. M. Zubarev, and O. V. Zubareva, Formation of curvature singularities on the interface between dielectric liquids in a strong vertical electric field. *Phys. Rev. E*, **88**(2), 023014 (2013).

[14] P. D. Lax, Development of singularities of solutions of nonlinear hyperbolic partial differential equations, *J. Math. Phys.* **5**(5), 611–613 (1964).

[15] J. R. Melcher and W. J. Schwarz Jr, Interfacial relaxation overstability in a tangential electric field, *Phys. Fluids* **11**(12), 2604–2616 (1968).

[16] D. W. Moore, The spontaneous appearance of a singularity in the shape of an evolving vortex sheet, *Proc. R. Soc. Lond. A* **365**(1720), 105–119 (1979).

[17] D. T. Papageorgiou, Film flows in the presence of electric fields, *Annu. Rev. Fluid Mech.* **51**, 155–187 (2019).

[18] D. T. Papageorgiou and O. Orellana, Study of cylindrical jet breakup using one-dimensional approximations of the Euler equations, *SIAM J. Appl. Math.* **59**(1), 286–317 (1998).

[19] D. T. Papageorgiou, P. G. Petropoulos, and J.-M. Vanden-Broeck, Gravity-capillary waves in fluid layers under normal electric fields, *Phys. Rev. E* **72**(5), 051601 (2005).

[20] B. Shraiman, & D. Bensimon, Singularities in nonlocal interface dynamics. *Phys. Rev. A* **30**(5), 2840–2843 (1984).

[21] G. I. Taylor and A. D. McEwan, The stability of a horizontal fluid interface in a vertical electric field, *J. Fluid Mech.* **22**(1), 1–15 (1965).

[22] B. S. Tilley, P. G. Petropoulos, and D. T. Papageorgiou, Dynamics and rupture of planar electrified liquid sheets, *Phys. Fluids* **13**(12), 3547–3563 (2001).

[23] Z. Wang, Modelling nonlinear electrohydrodynamic surface waves over three-dimensional conducting fluids, *Proc. R. Soc. A* **473**, 20160817 (2017).

[24] Z. Wang, Interfacial electrohydrodynamic waves under horizontal electric fields: Hamilton's principle and multi-scale modeling. *Advances in Mechanics*, in press (2022).

[25] V. E. Zakharov, Stability of periodic waves of finite amplitude on the surface of a deep fluid. *J. Appl. Mech. Tech. Phys.* **2**, 190–194 (1968).

[26] N. M. Zubarev, Exact solutions of the equations of motion of liquid helium with a charged free surface. *JETP*, **94**(3), 534–544 (2002).